Evaporation in capillary porous media at the perfect piston-like invasion limit: Evidence of non-local equilibrium effects

Alirez Attari Moghaddam, Marc Prat, Evangelos Tsotsas, Abdolreza Kharaghani

Evaporation in Capillary Porous Media at the Perfect Piston-Like Invasion Limit: Evidence of Nonlocal Equilibrium Effects

Alireza Attari Moghaddam[1], Marc Prat[2,3], Evangelos Tsotsas[1], and Abdolreza Kharaghani[1]

[1]Thermal Porcess Engineering, Otto-von-Guericke University Magdeburg, Magdeburg, Germany, [2]INPT, UPS, IMFT (Institut de Mécanique des Fluides de Toulouse), Université de Toulouse, Allée Camille Soula, Toulouse, France, [3]CNRS, IMFT, Toulouse, France

Key Points:
- The classical continuum modeling of evaporation in capillary porous media is revisited from pore network simulations
- The moisture diffusivity is characterized by a minimum corresponding to the transition between liquid and vapor transport mechanisms
- The pore network simulations indicate a noticeable nonlocal equilibrium effect

Correspondence to:
A. Kharaghani,
abdolreza.kharaghani@ovgu.de;
M. Prat,
mprat@imft.fr

Citation:
Attari Moghaddam, A., Prat, M., Tsotsas, E., & Kharaghani, A. (2017). Evaporation in capillary porous media at the perfect piston-like invasion limit: Evidence of nonlocal equilibrium effects. *Water Resources Research*, *53*, 10,433–10,449. https://doi.org/10.1002/2017WR021162

Abstract The classical continuum modeling of evaporation in capillary porous media is revisited from pore network simulations of the evaporation process. The computed moisture diffusivity is characterized by a minimum corresponding to the transition between liquid and vapor transport mechanisms confirming previous interpretations. Also the study suggests an explanation for the scattering generally observed in the moisture diffusivity obtained from experimental data. The pore network simulations indicate a noticeable nonlocal equilibrium effect leading to a new interpretation of the vapor pressure-saturation relationship classically introduced to obtain the one-equation continuum model of evaporation. The latter should not be understood as a desorption isotherm as classically considered but rather as a signature of a nonlocal equilibrium effect. The main outcome of this study is therefore that nonlocal equilibrium two-equation model must be considered for improving the continuum modeling of evaporation.

1. Introduction

The most commonly used approach for modeling evaporation in porous media approximates the porous medium by a continuum (Philip & De Vries, 1957; Sahimi, 2011) is often cited as the first who proposed a diffusion-based equation for the transport of moisture in porous media during evaporation incorporating the effects of capillary flow, vapor transport, and the coupling with heat transfer. Later on, in 1975, Luikov (1975) derived macroscopic equations governing the heat and mass transfer by volumetric summation of transport equations of each species based on the macroscopic flux relationships. A comprehensive model for heat and mass transfer during evaporation was developed by Whitaker (1977) within the framework of the volume averaging method, essentially confirming the model proposed by Philip and De Vries. For the simple drying situation considered in the present paper, namely the slow evaporation of a nondeformable capillary porous medium, Whitaker's model is still used nowadays—the corresponding set of equations is recalled later in this paper. Like any other continuum model, the continuum models for evaporation involve a set of medium-specific properties describing the fluid transport phenomena (intrinsic permeability, relative liquid and gas permeability, vapor diffusivity) and local equilibrium properties (capillary pressure and desorption isotherm). For a given porous medium, they must be specified as input parameters. Although widely used, these models cannot be considered as truly predictive and they have major shortcomings. The mass transfer at the interface between the porous medium surface and the bulk air is generally achieved by introducing a coefficient of mass transfer toward the surroundings. Using the well-known expressions for this coefficient, for example, Bird et al. (1960), rarely lead to good results because of the variations in the vapor partial pressure distributions over the surface during drying resulting from the coupling between the external and internal mass transfer, for example, Prat (1991). Therefore, this coefficient is often used as a fitting parameter. This is not satisfactory, however, because reproducing experimental data by use of fitting parameters is not a prediction. Another puzzling aspect lies in the introduction of a so-called desorption isotherm to link the saturation and the vapor partial pressure. Invoking adsorption-desorption phenomena makes sense for hygroscopic materials, that is, materials with a significant fraction of pores smaller than 1 μm, but can be questioned for capillary porous media, defined as porous media with pore sizes typically in the range of 1–100 μm. In other words, we believe that the classical continuum model of evaporation is not as firm as often considered and needs further investigation.

The idea for assessing the continuum model (CM) is simple: we consider a numerical model porous medium, namely a discrete pore network (PN), and perform PN simulations of evaporation which play the role of experiments. In other words, we take the PN model for granted and explore the ability of the continuum model to predict the results of the PN simulations of evaporation. Naturally, it is not claimed that the PN model perfectly reproduces the evaporation process in porous media. However, on the basis of comparisons with micromodel experiments presented in previous works, for example, Laurindo and Prat (1996, 1998) and Prat (2007), we think that the PNM model captures sufficiently key elements of the process to make the comparison with the CM interesting and instructive. The drying situation we consider corresponds to a typical laboratory experiment where the vapor forming as a result of evaporation escapes through the top surface of a porous sample. From the continuum standpoint, this is a one-dimensional situation, whereas the situation is of course three-dimensional as far as the PN simulations are concerned. Drying is slow, which means that the cooling effect due to evaporation can be neglected. Thus, the temperature is considered as uniform and constant throughout the drying process. For this reason, additional equations for heat transfer and for the air are not solved.

As discussed, for example, in Hoogland et al. (2016), invasion of the network first results from the piston-like displacement of the liquid by the gas in the throats and pores. However, some liquid often remains in the corners of the pores and throats, which are invaded by the gas phase in their center. As a result, the progressive displacement of the liquid by the gas phase can lead to the formation of a corner flow network in the region of the system where gas has already filled the center of the pores and throats. In the present work, the formation of such corner flow networks is neglected. In other terms, the liquid is assumed to be completely expelled from the pores or the throats during the piston-like displacement leading to the invasion of the pores and throats by the gas phase. For this reason, the considered drying process is referred to as evaporation in the perfect piston-like invasion limit. However, as shown in previous works, for example, Chauvet et al. (2009) and Yiotis et al. (2012), the impact of corner flows on evaporation can be quite important. Consequently, the corner film question will be discussed in relation with our results later in this work.

Although pore network drying models are being developed for more than 20 years now, they have not been used so far as a tool for assessing the continuum model. One a priori obvious reason is that the network size (i.e., the number of pores along each space direction) is typically relatively small owing to computational limitations. As a result, it is difficult to impose a significant length scale separation (the size of a representative elementary volume (REV) is actually not significantly smaller than the whole pore network), which is in principle a requirement for the continuum model to be accurate. In spite of this issue, as discussed in section 6, we believe that a comparison between pore network simulations and continuum model simulations is instructive and can bring valuable insights regarding the continuum modeling of evaporation in capillary porous media. This is the main objective of the present paper.

The paper is organized as follows: the CM is briefly recalled in section 2 and the model equations are given in detail in Appendix A. The pore network drying algorithm is briefly outlined in section 3. Two methods for determining the moisture transport coefficient for the CM from PN simulations are presented in section 4. The main simulation results are presented in section 5. A discussion is presented in section 6. The main conclusions are summarized in section 7.

2. The Continuum Model

The widely accepted continuum model of drying (Perré & Turner, 1999) is simplified to isothermal conditions and uniform and constant gas pressure, hence bringing it to the same level as the PN model described in section 3. In this CM, both liquid and gas phases coexist in the entire porous medium and corresponding mass transport is considered to be dominant in the direction perpendicular to the evaporative surface, which is named the z direction. The CM model can thus be simplified to the following single nonlinear partial differential equation for S

$$\varepsilon \frac{\partial S}{\partial t} = \frac{\partial}{\partial z}\left[D(S)\frac{\partial S}{\partial z}\right], \tag{1}$$

where ε, S, and t denote the porosity, liquid saturation ($0 < S \leq 1$) and time, respectively. Here the moisture transport coefficient D(S) is composed of two contributions, which are responsible for the moisture transport in the liquid phase, D_ℓ, and in the gas phase, D_v,

$$D(S) = D_\ell(S) + D_v(S). \tag{2}$$

The saturation-dependent function D(S) as well as the initial and boundary conditions need to be known in order to solve equation (1). It is assumed that the porous medium is initially filled with liquid water. At the bottom of the medium (z = 0), a zero-flux boundary condition is applied. At the evaporative surface of the medium (z = H), a boundary layer type relationship is considered to calculate the evaporation rate, namely

$$\dot{m}_v = \frac{\tilde{M}_v A}{\tilde{R}T} D_{va} p_v^* \left(\frac{\varphi(S) - \varphi_\infty}{\delta} \right), \tag{3}$$

where $\tilde{M}_v$ denotes the molar mass of vapor, A the surface area, $\tilde{R}$ the universal gas constant, T the air temperature, D_{va} the vapor molecular diffusion coefficient, p_v^* the saturation vapor pressure, and δ the boundary layer thickness. The function $\varphi(S)$ is classically considered as the desorption isotherm of the medium. For a given gas (water vapor in our case), the desorption isotherm is supposed to be a property of the porous medium and thus an input quantity for the CM. However, as we shall see (section 5.2), our interpretation of φ will be completely different.

The two parameter functions D(S) and φ(S) will be estimated from pore network simulations (see section 4 and Appendix A). The above set of model equations is solved using a finite difference discretization in space and an explicit time stepping scheme with variable time step and uniform spatial grid (200 computational nodes in z direction). Note that the above model is referred to as a one-equation continuum model since it involves a governing equation for the single variable S—see Appendix A for more details. For an introduction to the concepts of one and two-equation continuum models, one can refer, for example, to Quintard and Whitaker (1993).

3. The Pore Network Drying Algorithm

The pore network model is defined on a three-dimensional regular lattice of pores and throats. The throats are cylindrical tubes connecting the pores. The throat radii are randomly drawn from a normal distribution with given parameters (mean and standard deviation). All throats are saturated and the liquid exists as free capillary water and forms only one continuous cluster when evaporation starts. Periodic boundary conditions are applied on the lateral faces of the network. The pore network is extended by a discretized boundary layer of constant thickness, which is responsible for the external mass transfer of vapor generated during the evaporation process. Evaporation occurs at the throats which are exposed to ambient air.

The pores are volume-less computational nodes where the variables of interest, namely the liquid pressure or the vapor partial pressure, are computed. Transport phenomena are described by one-dimensional approximations at the discrete level of pores and throats, for example, Poiseuille's law for the liquid viscous flow and 1-D Fick's law for the diffusive transport of the vapor (see equations (4) and (5) later in the paper). From the mass balance at each node, two linear systems are formed and solved numerically to obtain the vapor partial pressure in each gas pore (and in the boundary layer) and the liquid pressure in each liquid pore, respectively. Due to the consideration of viscous and capillary forces at the same time, an iterative procedure is used to determine the stationary and the moving menisci. Thus, the pore network model is dynamic. The evaporation process generally leads to the drainage of the active throats ("active" means a throat where a meniscus is moving). However, reimbibition can locally occur in a throat depending on the evolution of the liquid pressure field. Time steps forward when one meniscus throat empties or (re)fills at every moment during drying. In the next step, new quasi-stationary vapor and liquid flow problems are solved again.

As the result of the invasion by the gas phase, the liquid phase in the network splits up into clusters with different sizes during the drying process. For liquid flow, it is essential to track the hydraulic connectivity of the liquid phase. Therefore, the liquid and vapor transport calculations are considered for each cluster independently, which implies the need for labeling liquid clusters. To this purpose, a variant of the Hoshen-Kopelman algorithm (Metzger et al., 2006) is used. The cluster labeling continues until the network saturation reaches zero. Note that liquid films inside throats are not accounted for in this PN model. Also, as supposed here, the PN dries virtually isothermally and thus the viscous resistance to convective flow in the gas phase is neglected and constant pressure is assumed. More details on this PN drying algorithm can be found in Metzger et al. (2007a).

4. Methods for the Determination of Continuum Model Parameters From PNM Simulations

On one hand, the nonlinear parameters of the continuum model for evaporation in porous media have originally been estimated by using either phenomenological approaches (Schoeber, 1976) or inverse methods (Gómez et al., 2007; Marchand & Kumaran, 1994; Pel et al., 1996): drying experiments were carried out in Pel et al. (1996) and Schoeber (1976) and absorption experiments in Gómez et al. (2007), Marchand and Kumaran (1994), and Pel et al. (1996) to determine transient saturation profiles for a given porous material. These experiments are not only laborious since the saturation varies slowly during these processes, but also there exists some uncertainty in the measured data. Then, the moisture transport coefficient was obtained by solving an inverse problem. In drying, for instance, this coefficient was readily estimated with a sufficient accuracy but only for a certain range of saturation (Pel et al., 1996). The values of this coefficient at low and high saturation were determined as follows: at low saturation a receding drying front model equation was solved numerically, whereas an absorption experiment was conducted to extract values of this coefficient at high saturation.

On the other hand, the computation of macroscopic parameters can be considered as one of the main uses of PNM (e.g., Blunt et al., 2002; Lerdahl et al., 2000; Øren et al., 1998) to name only a few. Most of those works focus on the computation of the permeability k, the relative permeability k_r, and the capillary pressure curve p_c. Although dynamic effects can be considered (e.g., Joekar-Niasar & Hassanizadeh, 2011), the most conventional method consists in computing the time-dependent phase distribution using quasi-static invasion rules. This is consistent with the assumption of local capillary equilibrium underlying the classical continuum model of two-phase flow in porous media. As can be seen from equation (A10), the liquid diffusivity D_ℓ can be directly computed from k, k_r (liquid phase), and p_c. This use of PNM is also prominent in relation to drying (e.g., Nowicki et al., 1992; Vorhauer et al., 2010), but using 2-D pore networks. It is well known that the percolation properties of the two fluid phases are different in 2-D and 3-D systems. For this reason, the consideration of three-dimensional networks is actually mandatory. Also, the network over which the variables of interest are computed is supposed to be a representative elementary volume (REV), so it must be large enough.

Based on the above, we use two different methods for computing the macroscopic parameters for our model porous medium, that is, our pore network. The first is inspired from experimental methods. It is based on postprocessing of phase distributions at distinct times, which are obtained from PN simulations of drying, over multiple realizations of the pore space geometry. This method directly uses the PN drying simulations to give the internal and surface relationships between vapor pressure and saturation as well as the moisture transport coefficient as a function of saturation. The second method is based on the conventional PNM computation of k, k_r (liquid phase), and p_c on a cubic network (e.g., Blunt et al., 2002).Thus, the second method does not use the PN *drying* simulations. In this method, the moisture transport coefficient is thus obtained through the computation of permeability, wetting fluid relative permeability, and capillary pressure using capillary-controlled invasion PN simulations and equation (A8). Whereas the first method allows to determine the variation of D over the full range of saturation, it can be noted that the second method allows the computation of the liquid diffusivity D_ℓ only and only for the saturations greater than the irreducible saturation.

4.1. Method #1: Pore Network Drying Simulations

The results of the PN drying simulations (i.e., nodal liquid and vapor pressure values as well as liquid distributions over time) are used to determine both the internal and the surface relationships between vapor pressure and saturation as well as the moisture transport coefficient. This method is described as follows: a three-dimensional pore network is divided into horizontal slices with constant thickness Δz at distinct times during the drying process. For illustration purposes, a small pore network and a partially saturated slice are shown in Figure 1. The slices are used as averaging volumes for determining local macroscopic variables, such as the average vapor partial pressure or the saturation. More precisely, in order to obtain the internal relationship between vapor pressure and saturation, the local saturation during the course of drying is calculated as a ratio of the liquid volume in an x-y plane of horizontal throats plus half of the vertical throats connected to this plane and dividing it by the pore space volume in this plane. Under isothermal conditions, the saturation vapor pressure is constant. The local mean vapor partial pressure is defined as the

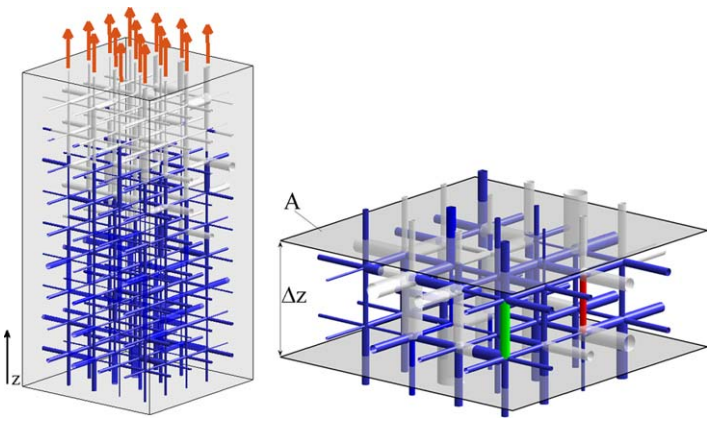

Figure 1. (left) A small pore network (6 × 6 × 11 nodes) open to evaporation from the top and (right) a slice (6 × 6 × 2 nodes) which is virtually cut out from the pore network. Exemplary liquid and gas throats spanning the slice are shown in green and red, respectively. A and Δz are the cross section of the network and the slice thickness, respectively.

arithmetic mean of the vapor pressures in the pores of each x-y plane. Likewise, the surface relationship between vapor pressure and saturation is built based upon variation of these properties over time in the top plane near the network surface.

The moisture transport coefficients for the liquid and gas phases (see equations (A10) and (A11)) are determined for each slice in the following way: knowing the nodal liquid pressures within each slice the liquid flow rate j_ℓ between pores i and k is calculated by using the Hagen-Poiseuille equation as

$$j_\ell = \frac{\pi r_t^4 \rho_\ell}{8\mu_\ell L_t}(p_{\ell,i} - p_{\ell,k}), \tag{4}$$

where L_t and r_t denote the length and radius of the throat, respectively. Then the liquid flux through each slice J_ℓ is obtained by summing the j_ℓ values over all vertical throats and dividing by the cross-sectional area of the sample A—see Figure 1. Disconnected clusters can contribute to J_ℓ if they expand over the slice height, although they might not contribute to the macroscopic liquid conductance. The moisture transport coefficient in the gas phase is calculated analogously. Different values of the vapor partial pressure at pores i and j may lead to vapor transport in the gas phase. For all vertically neighboring gas pores, the vapor flow rate through each slice is calculated by using the linear gas diffusion equation as

$$j_v = \frac{\pi r_t^2 \tilde{M}_v D_{va}}{\tilde{R} T L_t}(p_{v,i} - p_{v,k}). \tag{5}$$

Then, the vapor flux through each slice J_v is calculated and fed into equation (A11) to obtain the moisture transport coefficient of the vapor.

4.2. Method #2: Capillary-Controlled Invasion PN Simulations

A 25 × 25 × 25 cubic network is considered. This size was selected so that no noticeable change in the relationship between two-phase flow parameters and saturation is observed using bigger networks. A gas reservoir is located at the top of the network, whereas the liquid inside the porous medium is connected to a liquid reservoir at the bottom. Periodic boundary conditions are applied on the lateral faces of the network. The gas phase invades the network, which leads the liquid phase to be discharged from the network to its reservoir. The algorithm for building the relationship between capillary pressure and saturation from the capillary-controlled invasion simulations is as follows:

1. For simplicity and without affecting the final capillary pressure-saturation relationship, the liquid pressure in the network and in the liquid reservoir are set to zero. Therefore, according to equation (A4), the capillary pressure is equal to the gas pressure.
2. The smallest capillary threshold between all menisci is calculated. Here a perfect wetting between liquid and solid is considered (the wetting coefficient is unity), therefore the smallest capillary threshold according to the Young-Laplace equation belongs to the largest meniscus since
$$p_c = \frac{2\sigma}{r_t}, \tag{6}$$
where σ denotes the liquid surface tension.
3. The gas pressure, which is equal to the capillary pressure, is increased to the smallest capillary threshold calculated in step 2 to invade the menisci with the smallest capillary threshold.
4. The newly created menisci are identified and their capillary thresholds are calculated. If the capillary pressure is bigger than the capillary threshold of any of them, they are also invaded.
5. The saturation of the network is calculated and assigned to the capillary pressure. This is one data point in the capillary pressure-saturation curve.
6. The algorithm is repeated from step 2.

Invasion of gas into the liquid phase splits the continuous liquid phase into several disconnected clusters of different sizes, some of which are no longer connected to the liquid reservoir at the bottom of the network (trapped clusters). The process continues until there are no more connected clusters. The saturation of the network at this point is called irreducible saturation S_{irr}.

For the extraction of D_ℓ using equation (A8), k and k_r should still be determined. The procedures to obtain these two parameters are as follows: the network saturation is set to unity and then a liquid pressure difference is applied between two opposite sides of network. Thus the liquid pressure field inside the network is calculated and used to obtain the liquid flux in the network. By using equation (A2) and assuming $k_r = 1$, the intrinsic permeability is calculated. To estimate the relative permeability, a similar procedure as for k is used to calculate the liquid flux. This calculation is performed at each step of the capillary-controlled invasion process and as long as there is still connection between liquid at the top and bottom of the network. Then equation (A2) is employed.

5. Simulation Results

Using the two methods described in the previous section the macroscopic parameters and parameter functions are computed. The numerical values of these parameters are then used in the one-equation CM of drying; finally, the evolution of continuous saturation profiles and drying rate curves over time are compared to corresponding results obtained from the discrete PN drying simulations. The relevance of the CM is thus assessed.

5.1. Drying Kinetics

Due to computational limitations, pore network drying simulations are carried out on a relatively small cubic network with throat radii distributed according to a Gaussian distribution. In order to reduce the level of uncertainty on the parameter estimates, 15 realizations of the pore network were generated. The liquid is free capillary water and the drying agent is air with zero (absolute) humidity. The structural characteristics of PN and the physical constants for the simulations are given in Table 1. Since the CM accounts for the viscous flow driven by differences in capillary pressure (equation (A2)) in the partially saturated region, PN drying simulations are carried out in the presence of noticeable viscous effects in the liquid phase. Owing to the small size of our pore network, this requires the use of a rather unrealistic value for the liquid viscosity in order to stabilize the drying front, that is, such that the thickness of the two-phase zone is smaller than the network height over a significantly long period of drying. Expressed in terms of characteristic lengths (e.g., Lehmann et al., 2008), this means that the selected value of the viscosity leads to a viscous dissipation characteristic length smaller than the network height. This corresponds to an initial capillary number of 0.014, according to the formula given in Metzger et al., (2007b). This drying regime, where the two-phase zone is stabilized by the viscous effects, that is, the pressure drop generated in the liquid phase, is referred to as the viscous-capillary regime. For more details on the various drying regimes, one can refer to Prat (2002).

Figure 2 shows the evolution of the network saturation over time during the entire drying period and the corresponding normalized evaporation rate as a function of the network saturation. From the very beginning of the drying process, the network saturation decreases markedly because of relatively strong liquid viscous effects. Due to viscous stabilization, no first drying period is observed in these simulations. As the evaporation continues, liquid flow distances become longer and thus the differences in capillary pressure

Table 1
Structural Characteristics of the Pore Network and Physical Constants Used for Drying Simulations

Structural property	Value	Physical constant	Value
Network size (node)	$25 \times 25 \times 51$	Temperature (K)	293.15
Boundary layer discretization (node)	$25 \times 25 \times 10$	Pressure (Pa)	10^5
Mean throat radius (μm)	250	Liquid viscosity (m^2/s)	0.028
Standard deviation of throat radius (μm)	25	Surface tension (N/m)	0.07274
Throat length (mm)	1	Diffusion coefficient (m^2/s)	2.5685×10^{-5}
Network porosity	0.594	Saturation vapor pressure (Pa)	2,339

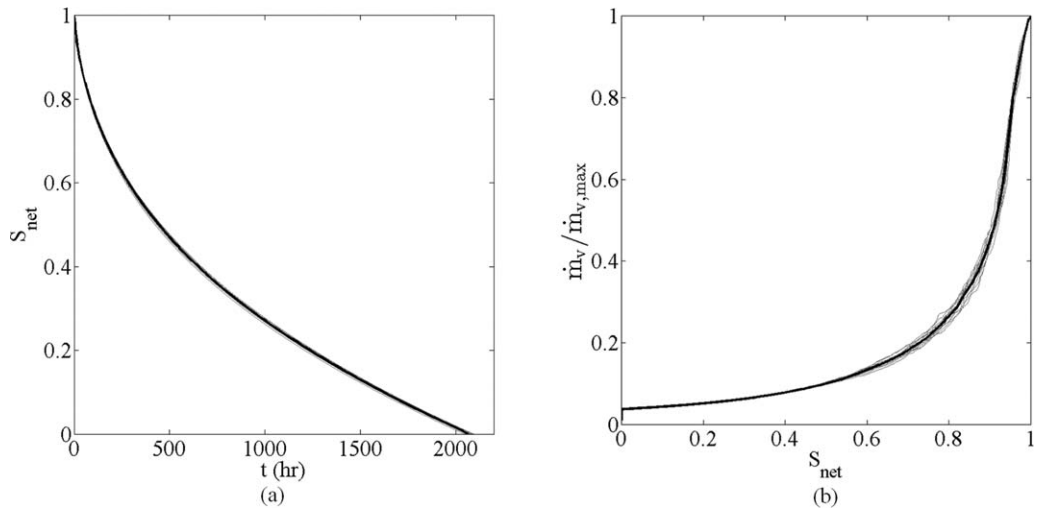

Figure 2. (a) Change of the network saturation and (b) of the normalized evaporation rate during drying. All 15 realizations and the arithmetic mean are shown in gray and black, respectively.

are insufficient to replenish the pores near the network surface by liquid water which evaporates at the high local rates. As a result, the evaporation rates are significantly reduced. With further decreasing evaporation rate, the gradient in network saturation is further reduced and the local saturation approaches the limit of liquid disconnection.

5.2. Relationship between Vapor Pressure and Saturation: Nonlocal Equilibrium Effect

Figure 3 shows the variation of the local mean vapor partial pressure and local saturation along the normalized height of the network obtained from the PN drying simulations at a network saturation of 0.75. As can be seen, the average vapor pressure is different from the saturation vapor pressure in the presence of liquid over a noticeable range of the local saturation, between 0.8 and 1. Since adsorption-desorption phenomena have been neglected in our numerical model porous medium, it is clear that the lower vapor pressure in the presence of liquid, that is, at nonzero saturation, has a different physical origin. It is, instead, interpreted here as the signature of a nonlocal equilibrium (NLE) effect. In the framework of the continuum approach to porous media, NLE means that the local thermodynamic equilibrium is satisfied at the menisci surface (where the vapor pressure is thus the saturation vapor pressure) but not at the scale of the averaging volume, that is, the averaging slices in our case. In other words, NLE means here that the slice-averaged vapor partial pressure is different from the saturation vapor pressure in the presence of liquid within the slice. This is an important difference from the conventional presentation of the continuum model. Here the function $\varphi(S)$ is therefore not interpreted as a desorption isotherm but as a NLE relationship.

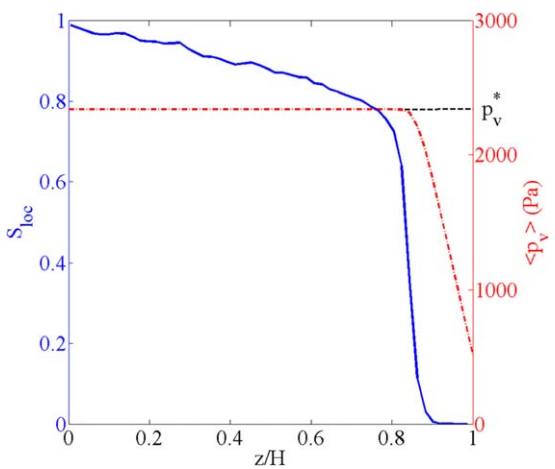

Figure 3. Profiles of the slice-averaged vapor partial pressure ($<p_v>$) and the local saturation (S_{loc}) over the normalized network height (z/H) obtained from the PN drying simulations at network saturation 0.75. Both properties are averaged over 15 realizations of a 25 × 25 × 51 network.

Figure 4 shows the values of internal NLE function (φ) averaged over small local saturation intervals (0.005) for different values of the network saturation. It can be seen that the functional dependency of φ on the local saturation varies during drying. Thus, a unique function $\varphi(S)$ cannot be identified over the whole drying process. The values of φ approach unity as the network saturation reaches zero. The reason is that in the low network saturation range, that is, $S_{net} = 0$–0.4, the liquid phase splits up into clusters with almost uniform lateral distribution in the two-phase region, whose thickness gradually increases as the liquid phase travels further into the network. This can be examined by calculating the ratio of saturation of isolated single meniscus throats to the network saturation, ξ, as shown during the drying process in Figure 5. One can clearly see that the contribution of isolated

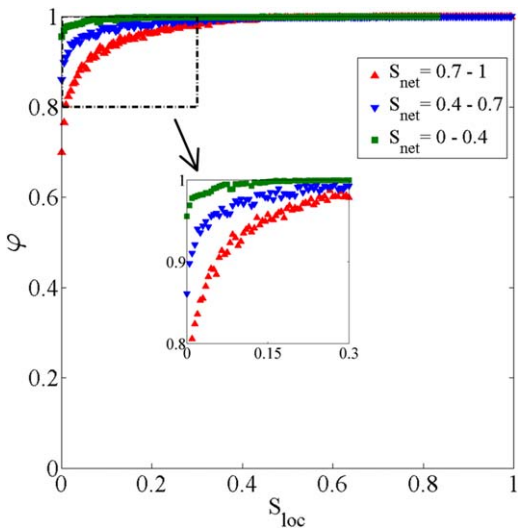

Figure 4. Mean value of internal NLE function (φ) obtained from the PN drying simulations as a function of local saturation (S_{loc}) for different network saturation (S_{net}) intervals.

single meniscus throats to the network saturation increases during evaporation and it drops substantially at the end of the drying process. Such a disintegration of the liquid structure inside the network at low saturation leads to higher vapor pressure values in the gas pores. Therefore, the mean vapor pressure reaches the saturation vapor pressure.

The PN drying simulations indicate that a NLE effect is also present at the network surface. The NLE function at the surface $\varphi_{surf}(S_{surf})$ is shown in Figure 6. Comparing these results with $\varphi(S)$ (Figure 4), it is clear that these two functions are different, although they follow a similar trend. The smaller values of φ_{surf} than φ at a given saturation are due to the fact that at the surface the vapor pressure is directly affected only by the liquid in the first layer of the network, whereas the vapor pressure values of the nodes inside the network are influenced by the liquid at their top and bottom layers. Therefore, for a given layer saturation, the vapor pressure at the surface is expected to be smaller than at any other position inside the network. This is also a noticeable departure from the conventional continuum modeling of drying, which is based explicitly on the local equilibrium (LE) assumption through the consideration of the "desorption isotherm" and on the implicit assumption that the "desorption isotherm" is still valid at the surface.

5.3. Moisture Transport Coefficient From Method #1

The moisture transport coefficients for the gas phase, D_v, for the liquid phase, D_ℓ, as well as for both phases, D, are obtained from the PN drying simulations (Figure 7). The results show that these three coefficients depend on the network saturation for local saturation $S_{loc} < 0.68$. Note that the local saturation is calculated here as the arithmetic mean of the saturation in two consecutive horizontal planes in each slice which consists of $25 \times 25 \times 2$ computational nodes. For $S_{loc} > 0.68$, the functional dependence of D_ℓ and D on network saturation is not clear though. The large variation observed in the data points is due to the fluctuations of the liquid pressure in the networks (Figures 7b and 7c). In this range of S_{loc}, the mean local vapor pressure is close to the saturation vapor pressure in the entire network, and no vapor pressure gradient can thus be built. Therefore, the mass transport is through the liquid phase only. This can be confirmed by looking at the ratio of local liquid flux, J_ℓ, over total local flux, J, shown in Figure 8. For $S_{loc} > 0.68$, $J_\ell / J = 1$, therefore the vapor flux is zero. By decreasing the local saturation, the vapor partial pressure in gas pores deviate from the saturation vapor pressure and more paths for the vapor transport become available, which leads to a stronger contribution of the transport in the gas phase to the total flux and thus D_v increases. The increase in D_v by reducing the local saturation can also be clarified by the NLE function φ data, shown in Figure 4. As can be seen, the derivative of φ over S_{loc} becomes larger as the local saturation decreases, which results in a larger value of D_v (equation (A11)).

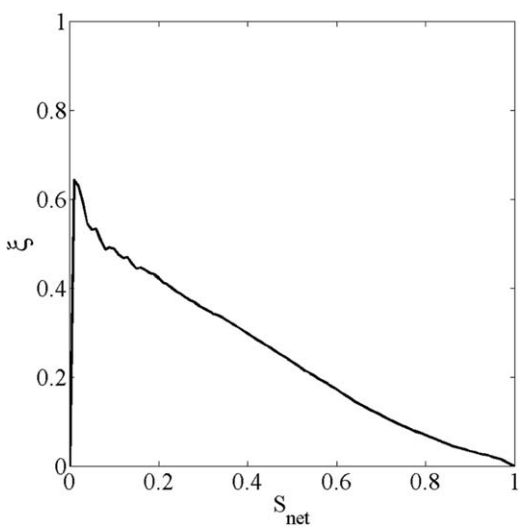

Figure 5. Ratio of saturation of isolated single meniscus throats to the network saturation during drying (ξ), averaged over 15 realizations of a network of $25 \times 25 \times 51$ nodes.

It is clear from Figure 7a that at a certain local saturation D_v decreases as the network saturation reduces. This behavior can be explained by noting how ξ changes over drying time (Figure 5). At low S_{net}, the relative amount of isolated throat saturation is bigger and the fragmented liquid is more uniformly distributed. Therefore, when going from one layer to its neighboring layer the vapor pressure is expected to be smoother, which leads to a smaller vapor flux and smaller D_v. The deeper position of the drying front at lower S_{net} is also a reason for the reduction of D_v.

At $S_{loc} = 1$, the hydraulic conductivity of the liquid is at its maximum, therefore the moisture transport coefficient in the liquid phase has

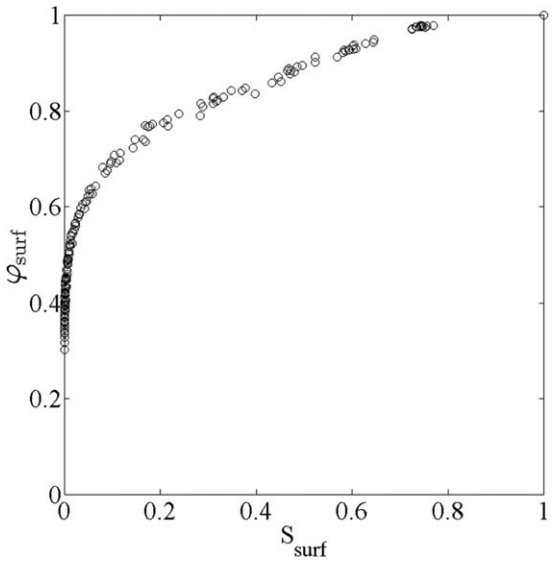

Figure 6. Mean value of external NLE function (φ_{surf}) versus the network surface saturation (S_{surf}) obtained from the PN drying simulations.

the highest value. By decreasing the local saturation, the continuity of the liquid phase is affected and thus D_ℓ is reduced. For $S_{loc} < 0.68$, the liquid pressure profile has developed and the dependency of D_ℓ on the network saturation becomes clear. As for D_v, the dependency of D_ℓ on the network saturation can be explained by the presence of isolated menisci. At high S_{net}, the liquid predominantly remains in the main cluster making the transport of liquid easier. This results in a higher liquid flux and moisture transport coefficient. However, at low S_{net}, the contribution of the isolated menisci to the network saturation is bigger (Figure 5), thus a smaller part of liquid can effectively contribute to the liquid transport and, consequently, D_ℓ will be lower. That also explains the dependence of the transition point between dominant phases for the transport on S_{net}. This point corresponds to the saturation at which $J_\ell/J = 0.5$ and represents equal contributions by the gas and liquid phases to the transport. With decreasing S_{net}, which leads to an increasing number of isolated menisci, the local saturation at which the transition happens becomes bigger.

As can be seen in Figures 7b and 7a different behavior of D_ℓ at different network saturation intervals is observed when $S_{loc} < 0.2$. When S_{loc} decreases to values smaller than 0.2, the moisture transport coefficient in the liquid phase increases with a decreasing saturation at low network saturation, whereas the opposite behavior is observed at higher network saturation. Since the majority of liquid in the latter case is in the main cluster, decreasing the local saturation leads to lowering the effective paths for the transport of liquid. This consequently leads to the reduction of the moisture transport coefficient in the liquid phase. However, at lower network saturation, for $S_{loc} < 0.2$, it is more likely that by decreasing the local saturation, the amount of isolated menisci is reduced, because they compose the larger part of liquid. This means that the effective paths for the transport of liquid may stay almost unchanged. Knowing that the spatial gradient of the saturation decreases by decreasing the local saturation below 0.2 (see Figure 12) and assuming that J_ℓ stays constant in this range, then according to equation (A10) D_ℓ should increase.

The total moisture transport coefficient, that is, $D = D_v + D_\ell$, is shown in Figure 7c. For all network saturation, a minimum in D is observed. The local saturation at which this minimum occurs (S_{min}) is almost equal to the transition saturation at which $J_\ell/J = 0.5$ (Figure 8). In the region with saturation higher than S_{min}, the liquid transport is more significant (D_ℓ is bigger), while at lower local saturation vapor transport plays a more important role (D_v is bigger). Interestingly, the trends depicted in Figure 7 are in a qualitative agreement with the experimental determination of D, D_v, D_ℓ for a sand sample reported in Crausse et al. (1981). The existence of the minimum illustrated in Figure 7c is in agreement with the results of Crausse et al. (1981) as well as with similar results reported for various porous materials (e.g., Pel et al., 1996). In agreement with previous works (e.g., Pel et al., 2002, and references therein), our simulations thus confirm that the minimum corresponds to the transition between liquid and vapor transport mechanisms.

5.4. Single-Phase and Two-Phase Flow Parameters From Method #2

The capillary-controlled invasion simulations were performed on 45 realizations of a $25 \times 25 \times 25$ network, which was artificially cut out of the original pore network in a random way. The computed value of the intrinsic permeability is $1.6 \times 10^{-9} \pm (7 \times 10^{-13})$ m^2.

The data points obtained from all realizations for the capillary pressure and relative permeability versus the local saturation are shown in Figure 9. Here as well as in Figure 10, local saturation refers to the network saturation. The irreducible saturation obtained from the capillary-controlled invasion simulations is $0.68 \pm (4 \times 10^{-4})$ and that is the reason why there is no data for saturation smaller than that in these curves. The unusually high irreducible saturation is due to several factors: (1) the fact that perfect trapping rules are used (e.g., Joekar-Niasar et al., 2008), (2) the fact that the pores are volume-less (the fluids are in the throats) in our pore network model, and (3) the fact that the standard deviation of the throat size distribution $\sigma_{rt} = 25$ μm is relatively small compared to the mean throat size ($\bar{r}_t = 250$ μm) as indicated in Table 1. For

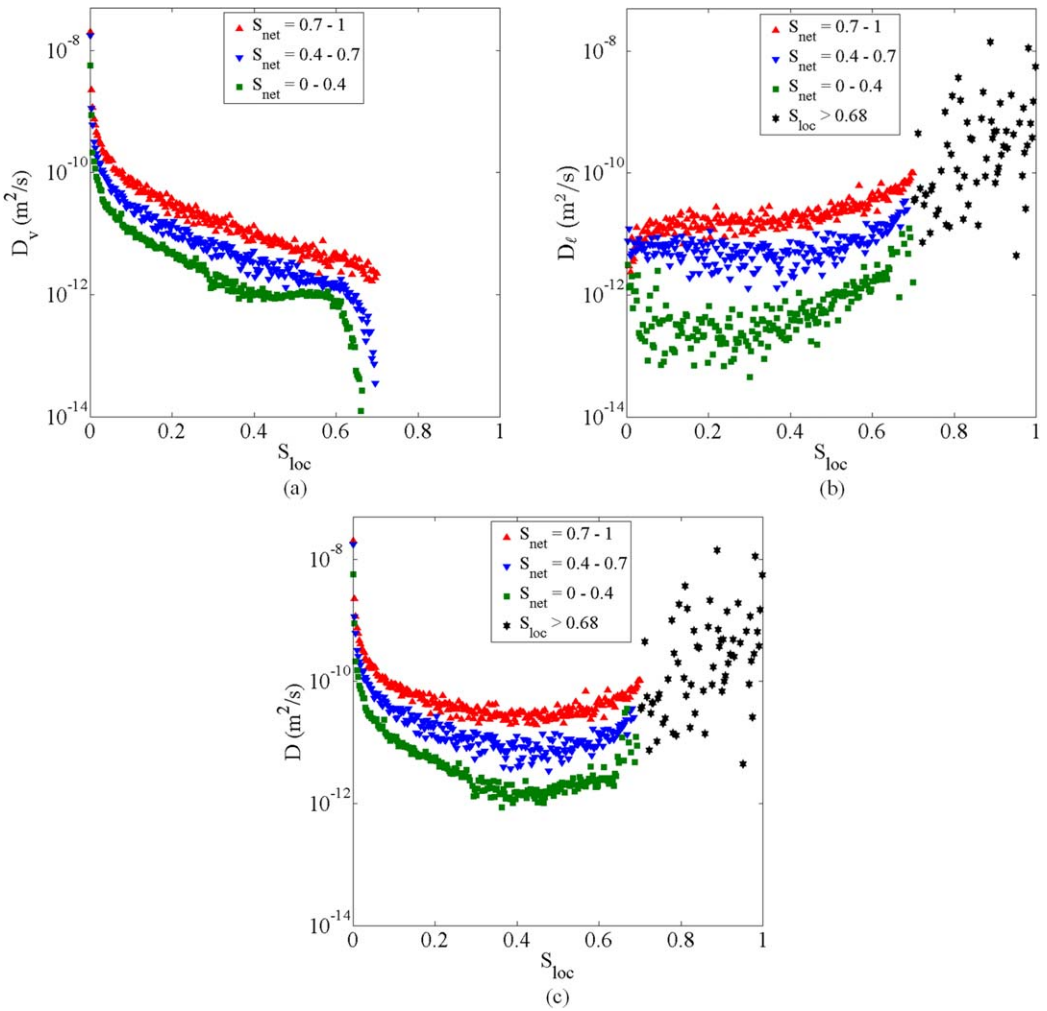

Figure 7. Moisture transport coefficients for the (a) gas and (b) liquid phases as well as (c) the total moisture transport coefficient obtained from the PN drying simulations. The values are averaged over local saturation intervals.

example, increasing the standard deviation from 25 to 140 μm while keeping the same mean throat size leads to a decrease in the irreducible saturation from 0.68 to 0.43. This is so because larger throats are preferentially invaded. Distributing the pore space volume over the throats and the pores (nodes) in the cubic network also reduces the irreducible saturation as can be seen in Le Bray and Prat (1999) where $S_{irr} \sim 0.45$. To sum up, the high irreducible saturation observed in our simulation is due to the consideration of perfect trapping rules, volume-less pores and a relatively weak disorder. Shifting the irreducible saturation toward a high value actually allows zooming over the range of saturations below the irreducible saturation with method #1. When the network is fully saturated, the capillary pressure is at its minimum and the conductivity of the liquid inside the network is completely established, meaning that the relative permeability is one. Bigger throats are invaded as the gas continues to invade the network, leading to an increase in the capillary pressure. This is followed by a reduction in the conductivity of the liquid, which consequently leads to a continuous decrease in the relative permeability, until no invasion is possible anymore.

For the estimation of the moisture transport coefficient D, actually D_ℓ, with method #2 the following procedure is taken: the whole saturation range (S_{irr} to 1) is split into small intervals of equal size. By averaging between all the values of the two-phase flow parameters in each interval, their average values corresponding to each interval are then obtained. The ratio of the capillary pressure difference over the mean local saturation difference between two consecutive intervals gives an approximation for the derivative dP_c/dS_{loc}. By using equation (A8) D_ℓ can be extracted. The results obtained by this method are shown in Figure 10.

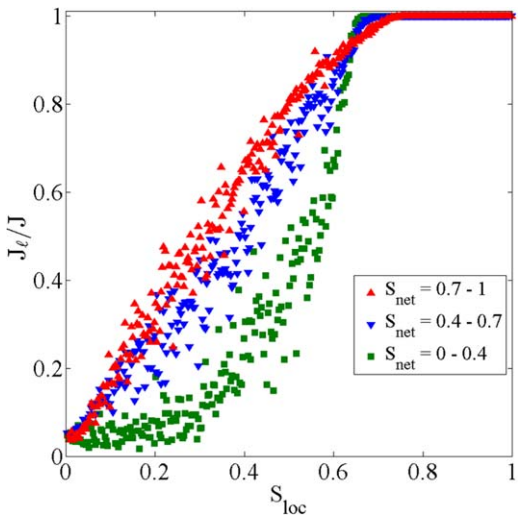

Figure 8. Ratio of the liquid flux over total flux during drying of the pore network at different network saturation intervals.

In spite of the quite significant scatters in both figures, it is concluded from the comparison of Figures 7 and 10b that the trends in the D_ℓ data points obtained from the two methods are in agreement, although their values for very high local saturation deviate somewhat from each other. We believe the scatters would be less, should we be able to perform the PN drying simulations over bigger networks. Since we consider averaging volumes of different sizes in method #1 and in method #2, we also interpret the similar trends regarding D_ℓ in Figure 7b and Figure 10 as an indication that the averaging volumes used in our work are consistent with the objectives of the paper (see the end of section 6 for further discussion on the choice of the averaging volume).

5.5. Comparison Between Continuum Model and Pore Network Simulation Results

The moisture transport coefficient D and the NLE surface function $\varphi = \varphi_{surf}$ obtained using method #1 are used to solve the one-equation continuum model (CM; equations (A8) and (3)). When solving these two equations, the local saturation can reach very small values, for which no values of D and φ_{surf} obtained from PN drying simulations are available. This is due to the fact that local saturation can be captured only until a certain positive value, therefore the values of these two parameters are unknown for very small local saturation. A solution may be to increase the network size, so that the aforementioned parameters can be calculated for lower local saturation. This solution however increases the computation time and might not solve the problem completely, since the local saturation in the CM could still become lower than the smallest saturation of the slice.

In order to obtain values of D at very low local saturation, the following method based on the evaporation rate obtained by PN drying simulations is used: after fitting a curve to the available data points of the moisture transport coefficient and NLE function at the surface φ_{surf}, the discretized one-equation continuum drying model is solved. When the surface saturation reaches very small values, for which D and φ_{surf} values are not available ($S_{surf} < 2 \times 10^{-4}$), the averaged evaporation rate from the PN drying simulations is applied as the boundary condition. Then the value of D for the corresponding surface saturation is obtained, provided that the mass conservation at the surface is satisfied. In this way, the moisture transport coefficient of any other node with $S < 2 \times 10^{-4}$ can be obtained. Then a curve is fitted through all data points of D. By applying the same procedure for the evaporation rate (using $\varphi_{surf}(S)$ to calculate the evaporation rate for

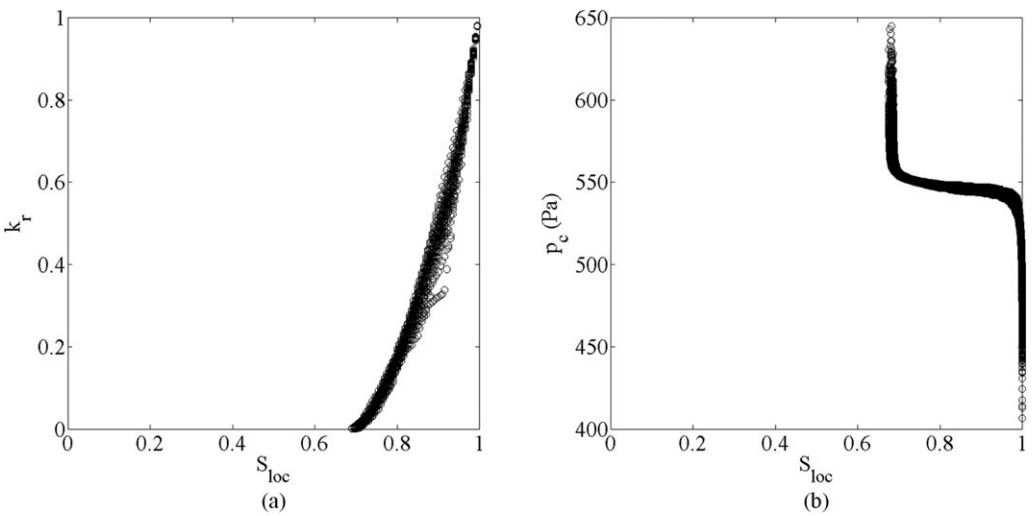

Figure 9. (a) The relative permeability and (b) the capillary pressure for a network of 25 × 25 × 25 nodes versus its saturation.

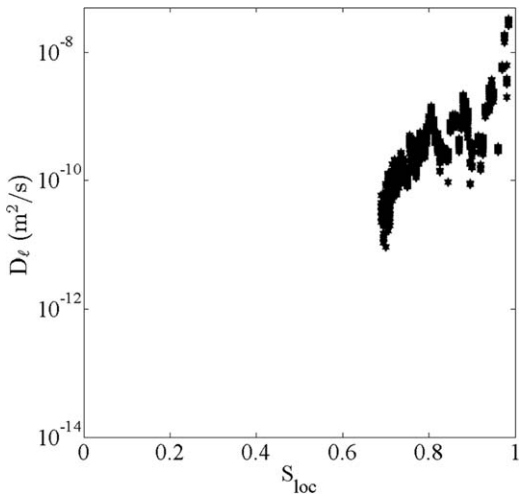

Figure 10. The moisture transport coefficient for the liquid phase obtained from the capillary-controlled invasion simulations.

$S_{surf} > 2 \times 10^{-4}$ and the averaged evaporation rate for the PN drying simulations for $S_{surf} < 2 \times 10^{-4}$) and using the new fitted curve for D, this time the CM can be solved until the network dries completely.

The normalized averaged evaporation rates computed by the CM (equation (3)) and PN drying simulations are shown in Figure 11. The evaporation rate is computed with the CM as long as data points of φ_{surf} are available ($S_{net} \sim 0.85$). Afterward, the evaporation rate of PN drying simulation is used as boundary condition in the CM. As can be seen, the evaporation rate curves resemble each other very well. This of course only shows that the CM model can reproduce the data and is by no means a proof that the CM model can predict the evaporation rate. This important point is further discussed below in the discussion section. The saturation profiles obtained from the two methods are plotted against the network depth in Figure 12. As can be seen, the CM is able to reproduce the saturation profiles of the PN simulations for drying over the full saturation range. However, there is a price that has to be paid for this agreement, namely that the local relative humidity of air has to be fitted as a function of the local saturation for both the interior of the material ($\varphi_{surf}(S)$) and its surface ($\varphi(S)$) (see Figures 4 and 6).

6. Discussion

Since the CM model is able to reproduce the PN simulation results, it is tempting to consider that the results presented in the previous section confirm the overall validity of the CM model. Accordingly, the main problem would be "simply" a correct determination of the macroscopic parameters. With the permanent progress in imaging techniques (X-ray microtomography, FIB-SEM, etc.) (e.g., Bultreys et al., 2016; Wang et al., 2012), and using techniques for constructing pore networks from digital images of microstructures (e.g., Agaesse et al., 2016), it would be just a matter of time to determine these parameters accurately from high-performance pore network computations. However, we believe that the conclusion one must draw from the results presented in section 5 is different, as discussed in the following paragraph.

Compared to the current state of the art concerning the CM for drying, the results presented in the previous section show several differences. The moisture transport coefficient function $D(S_{loc})$ is not unique, but depends on the network saturation (as illustrated in Figure 8). Indeed, we used three different functions depending on the average saturation of the medium. This was explained by the impact of isolated liquid throats whose relative fraction increases during the drying process. However, as already mentioned, the general shape of function D(S) is in qualitative agreement with experimentally determined functions (Crausse et al., 1981; Pel et al., 1996). More interestingly and more importantly in our opinion, the pore network simulations indicate a significant nonequilibrium effect, that is, the average vapor pressure is lower than the saturation pressure when the saturation is sufficiently low but non zero in the averaging volume (a horizontal slice containing one row of pores in our simulation). Also, we had to consider a NLE function at the surface, different from the one inside the network, and the NLE function inside the two-phase region was not unique. Even if we assume that repeating the work over much bigger pore networks would lead to a unique internal NLE function, the consequence would be that the present version of the CM for drying is intrinsically not adapted to model the drying process in our pore network. The existence of the NLE effect is a strong indication that a NLE two-equation model would be much more appropriate. Contrary to the classical CM, where the equations describing the transport in the liquid and vapor phases are combined

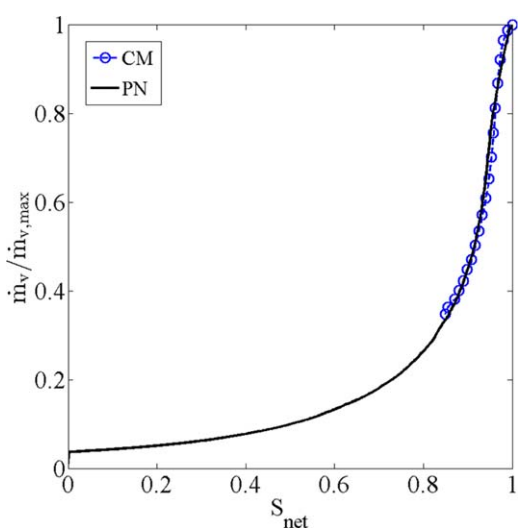

Figure 11. Normalized averaged evaporation rates predicted by equation (3) and by the PN drying simulations.

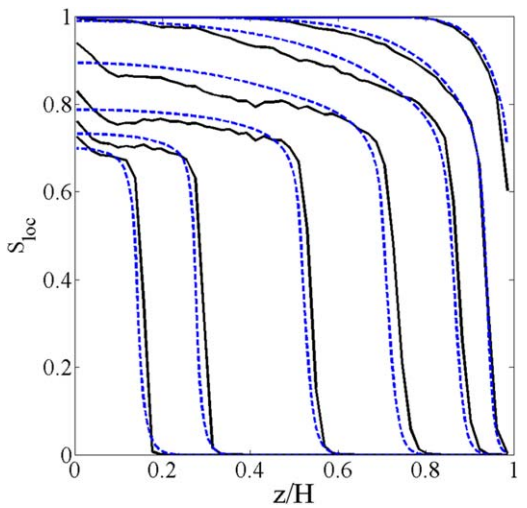

Figure 12. Saturation profiles obtained from the CM (blue dashed lines) and PN (black solid lines) simulations. The saturation profiles of PN are averages over 15 realizations. From top the profiles belong to network saturation of 0.98, 0.9, 0.8, 0.6, 0.4, 0.2, and 0.1, respectively.

to obtain a single transport equation, liquid and vapor transport would be kept separate in the two-equation model and a source-sink term, equation (7) below, would take into account the NLE exchange between the phases. Developed in the context of the volume averaging method (e.g., Quintard & Whitaker, 1993), a simplified version of the two-equation model assuming the liquid phase to be immobile is presented in Pujol et al. (2011). A heuristic but more comprehensive version is proposed, for instance, in He et al. (2000). In this type model, the evaporation rate $\dot{m}_v$ within a REV is expressed according to a NLE relationship of the form,

$$\dot{m}_v = \frac{\varepsilon S \rho_\ell}{\tilde{M}_v} \beta \left(p_v^* - p_v \right), \tag{7}$$

where β is the mass exchange coefficient. This parameter is a key parameter in the context of NLE models (e.g., Quintard & Whitaker, 1993; Pujol et al., 2011). The evaluation of this coefficient from PNM simulations of drying is the logical next step to continue the present work. It is important to realize that equation (7) has generally nothing to do with nonequilibrium effects at the scale of menisci as described for instance by the Hertz-Knudsen-Schrage equation (Barrett & Clement, 1992; Schrage, 1953). Although the Hertz-Knudsen-Schrage equation is mathematically analogous to equation (7), there is no need of nonequilibrium effects at the meniscus scale to observe NLE effects at the macroscopic scale. This is clearly illustrated by our PNM simulations that lead to NLE effects while the classical assumption of local thermodynamic equilibrium is made at the scale of each meniscus. This is so because the resistance to evaporation modeled by the Hertz-Knudsen-Schrage equation is generally negligible compared to the resistance associated with the diffusion transport of the vapor in the pore space.

The fact that the surface NLE function $\varphi_{surf}(S_{surf})$ is different from the internal NLE functions $\varphi(S)$ is interpreted as a strong illustration of the problem posed by the adequate description of the transfer at the surface, where the internal and external transfers must be coupled. The modeling of the transfer at the medium surface is often seen as the major problem of the theory of drying and the present results can be regarded as an additional confirmation that more work on this topic is needed.

Now there is the question of the representativeness of our pore network model compared to real systems. Since the main new aspect is the NLE effect, the question arises as to whether this effect might just be a consequence of the model. As discussed in Vorhauer et al. (2015), it is well established that secondary capillary structures can form during the invasion of the pore space by the gas phase as a result of evaporation. Secondary capillary structures refer to capillary bridges, rings, liquid films forming in wedges, contact regions between particles, constrictions and other geometrical singularities of the pore space. The formation of the secondary capillary structures strongly depends on the local geometry of the pore space and wettability properties (the lower the contact angle, the more likely the formation of secondary capillary structures). The formation of secondary capillary structures can be considered as taken into account in the pore network model used in the present paper since liquid can be temporarily trapped in single throats. However, from previous pore network simulations that take into account the corner flows (e.g., Prat, 2007; Yiotis et al., 2004) and experiments (Chauvet et al., 2009; Yiotis et al., 2012), it is known that the impact of corner films on evaporation can be very important. Thus, the case with major film effect can be considered as a different situation which needs a separate study, for instance, along the same lines as the present one but using the version of the drying PNM with films (e.g., Prat, 2007; Yiotis et al., 2004). In other terms, the impact of secondary capillary effects on the NLE effect in real systems therefore deserves to be studied. Since film effects are much more likely when the liquid is perfectly wetting or for low contact angles, it is expected that the case studied in the present paper could correspond to intermediate contact angles (sufficiently below 90° for the drainage displacement local rules to apply but sufficiently greater than 0° for the impact of corner films to be negligible).

To end this section, an important issue must be discussed. It is well known that the continuum model recalled in section 2 is based on a length scale separation assumption (e.g., Whitaker, 1997). In other words,

the averaging volume should be representative, that is, a REV. Thus, it should be large enough to be representative of the porous medium microstructure but small enough compared to the size of the porous domain for the macroscopic variables to be considered as local. For example, the results reported in Tahmasebi et al. (2017) suggest than the REV size of a sandstone measured using the mean throat size as unit is about 300! whereas the numerical results reported in Joekar-Niasar et al. (2008) for cubic networks indicated that the REV should contain about 40 pores in each coordinate direction. In the case of our relatively weakly disordered network, it was found that a network with 25 pores in each direction could be considered as a REV. This is why this size was selected for the computations presented in section 5.4. Thus, clearly, it can be argued that the traditional length scale separation criteria are not met in our approach since there are only a few slices over the network height and the slice thickness is of one lattice unit only (the lattice unit is the distance between two pores in the network). In this respect, the results would be more convincing if the simulations had been performed with variable network and averaging volume sizes. Increasing sufficiently the size of the network for the influence of the size to be assessed properly is not possible with our present version of the PN drying code due to computational times. On the other hand, it is known that the continuum model can be seen as an asymptotic model in the context of homogenization methods (e.g., Auriault, 2005). This can be interpreted as: the greater the length scale separation, the better the accuracy of the continuum model results is. Thus, here, it can be considered that we have simply accepted a low level of accuracy, which is illustrated for example by the scattering of the results in Figure 7. In other words, we believe that the trends and main results revealed by our simulations will be confirmed when simulations are performed over larger networks but this of course remains to be demonstrated.

Regardless of the results over bigger networks, the work presented in the present paper can also be considered as giving insights into the applicability of the conventional continuum model to simulate drying in thin systems, that is, systems characterized by a poor length scale separation over their thickness.

7. Conclusions

In this work, the results obtained from the one-equation continuum model and from pore network simulations for drying of a capillary porous medium are compared and assessed. The results for the moisture transport coefficient showed three critical points in the D-S curve: two maxima at opposing local saturation limits, which show that, when the transport is entirely in either the liquid phase ($S \sim 1$) or the vapor phase ($S \sim 0$) and a minimum that occurred at S_{min} when both types of transport are of comparable magnitude in good qualitative agreement with experimental determinations on real samples published in the literature. Our results confirm previous interpretations linking the moisture coefficient minimum to the transition between liquid and vapor transport mechanisms.

Contrary to previous works, however, three D-S curves were actually identified to describe the drying process with the continuum model. This was attributed to the impact of isolated liquid menisci that become increasingly more numerous for similar local saturation during the drying process. In other words, our simulations indicate a change in the local structure of the liquid phase along the drying process. This is in contradiction with the classical local capillary assumption implicitly stated through the use of a single retention curve (in drainage) that a unique liquid phase structure within the REV corresponds to each level in saturation. It can be argued that the fact that we did not obtain a unique function of saturation is due to the small size of our pore network, which implies a poor length scale separation between the averaging volume size and the sample size. However, we note that the experimental determinations of D-S as reported, for instance, in Pel et al. (1996, 2002) show a somewhat similar scattering with clouds of values for each saturation. Although further work is needed to clarify this issue, we propose, based on our results, to interpret the scattering as a sign of the nonunique correspondence during drying between the saturation and the local distribution of the liquid phase.

The main conclusion, however, is that the classical interpretation of the relationship between the vapor partial pressure and the saturation, which was introduced in the development of the one-equation model as a desorption isotherm, is wrong, at least for our model porous medium. This relationship is instead the signature of a nonlocal equilibrium effect. As a result, testing NLE two-equation model against drying PNM simulations is the logical next step to improve the continuum modeling of drying.

One should, however, keep in mind that the PNM used in the present work takes into account only perfect piston-like displacements at the throat/pore scale, thus neglecting the secondary capillary effects. Although we believe that NLE effects must be present in the presence of secondary capillary effects, at least in the transition region where the liquid in pendular state evaporates, this is at this stage a mere opinion. Work is needed to explore this issue and hopefully to transform this opinion into fact. Also, it would be desirable to repeat the simulations over much bigger networks because of the poor length scale separation in our simulations.

Appendix A

This appendix represents detailed equations of the continuum model discussed in section 2. Assuming quasi steady transfer of vapor in the gas phase, the one-dimensional CM for drying in a porous medium is given by the mass balance equation

$$\rho_\ell \varepsilon \frac{\partial S}{\partial t} = -\frac{\partial}{\partial z}[J_\ell + J_v], \tag{A1}$$

where ρ_ℓ denote the liquid mass density. The liquid flux J_ℓ is obtained from the generalized Darcy's law (neglecting gravity) under steady state conditions

$$J_\ell = -\rho_\ell \frac{k k_r}{\mu_\ell} \frac{\partial p_\ell}{\partial z}, \tag{A2}$$

where k, k_r, and μ_ℓ denote the intrinsic permeability, relative permeability, and dynamic viscosity of the liquid, respectively. Assuming that the binary gas mixture of vapor and air behaves like an ideal gas, the vapor flux is expressed by

$$J_v = -\frac{\tilde{M}_v}{\tilde{R}T} \frac{p_{atm}}{p_{atm} - p_v} D_{veff} \frac{\partial p_v}{\partial z}, \tag{A3}$$

where p_{atm}, p_v, and D_{veff} denote the atmospheric pressure, partial pressure of vapor and vapor diffusivity, respectively.

Invoking the local capillary equilibrium assumption, a relationship between liquid and capillary pressure is obtained by

$$p_c = p_{atm} - p_\ell. \tag{A4}$$

Combining equations (A1–A4), the continuum model can be written as:

$$\rho_\ell \varepsilon \frac{\partial S}{\partial t} = \frac{\partial}{\partial z}\left[\rho_\ell \frac{k k_r}{\mu_\ell}\left(-\frac{\partial p_c}{\partial S}\frac{\partial S}{\partial z}\right) + \frac{\tilde{M}_v}{\tilde{R}T}\frac{p_{atm}}{p_{atm} - p_v} D_{veff} \frac{\partial p_v}{\partial z}\right]. \tag{A5}$$

The first term on the right-hand side of equation (A5) describes the liquid transport in those regions of the porous medium where there is a nonzero saturation gradient in the liquid phase, whereas the second term represents the diffusive vapor transport in the regions where the gradient of the vapor partial pressure is nonzero.

In order to make the solution of equation (A5) easier, one possibility is to obtain a one-equation CM by introducing a relationship between the liquid saturation S and the vapor partial pressure p_v of the form

$$\varphi(S) = \frac{p_v}{p_v^*}. \tag{A6}$$

The one-equation CM can thus be parametrized as

$$\varepsilon \frac{\partial S}{\partial t} = \frac{\partial}{\partial z}\left[\left(\frac{k k_r}{\mu_\ell}\left(-\frac{\partial p_c}{\partial S}\right) + \frac{1}{\rho_\ell}\frac{\tilde{M}_v}{\tilde{R}T}\frac{p_{atm} p_v^*}{p_{atm} - p_v^* \varphi} D_{veff} \frac{\partial \varphi}{\partial S}\right)\frac{\partial S}{\partial z}\right]. \tag{A7}$$

The inner bracket of equation (A7) corresponds to the moisture transport coefficients of the CM, namely

$$D_\ell = \frac{k k_r}{\mu_\ell}\left(-\frac{\partial p_c}{\partial S}\right), \tag{A8}$$

$$D_v = \frac{1}{\rho_\ell}\frac{\tilde{M}_v}{\tilde{R}T}\frac{p_{atm}p_v^*}{p_{atm}-\varphi p_v^*}D_{veff}\frac{\partial \varphi}{\partial S}. \tag{A9}$$

Comparing equation (A7) with equation (A1), D_ℓ and D_v can be expressed as:

$$D_\ell = -\frac{1}{\rho_\ell}\frac{J_\ell}{\partial S/\partial z}, \tag{A10}$$

$$D_v = -\frac{1}{\rho_\ell}\frac{J_v}{\partial S/\partial z}. \tag{A11}$$

Equations (A10) and (A11) show that in the one-equation CM the driving force for transport in both the liquid and gas phases is the saturation gradient, which changes with time and position.

Acknowledgments

This work was financed by the German Research Foundation (DFG) within the Graduate School 1554 "Micro-Macro-Interactions in Structured Media and Particulate Systems". Also, partial financial support from joint project "Drycap" funded by GIP ANR (project 16-CE92-0030-01) and DFG (project TS 28/10-1) is gratefully acknowledged. Our paper is theoretical and the data can be found in Attari Moghaddam (2017). The final manuscript benefited from constructive comments given by the Associate Editor and three anonymous referees; we greatly appreciate their efforts.

References

Agaesse, T., Lamibrac, A., Büchi, F. N., Pauchet, J., & Prat, M. (2016). Validation of pore network simulations of ex-situ water distributions in a gas diffusion layer of proton exchange membrane fuel cells with X-ray tomographic images. *Journal of Power Sources*, *331*, 462–474. https://doi.org/10.1016/j.jpowsour.2016.09.076

Attari Moghaddam, A. (2017). *Parameter estimation and assessment of continuum models of drying on the basis of pore network simulations*. (PhD thesis). Magdeburg, Germany: Otto-von-Guericke University.

Auriault, J.-L. (2005). Transport in porous media: Upscaling by multiscale asymptotic expansions. In L. Dormieux & F.-J. Ulm (Eds.), *Applied micromechanics of porous materials* (pp. 3–56). New York, NY: Springer.

Barrett, J., & Clement, C. (1992). Kinetic evaporation and condensation rates and their coefficients. *Journal of Colloid and Interface Science*, *150*(2), 352–364. https://doi.org/10.1016/0021-9797(92)90205-Z

Bird, R. B., Stewart, W. E., Lightfoot, E. N. (1960). *Transport phenomena*. New York, NY: Wiley.

Blunt, M., Jackson, M. D., Piri, M., & Valvatne, P. H. (2002). Detailed physics, predictive capabilities and macroscopic consequences for pore-network models of multiphase flow. *Advances in Water Resources*, *25*, 1069–1089. https://doi.org/10.1016/S0309-1708(02)00049-0

Bultreys, T., De Boever, W., & Cnudde, V. (2016). Imaging and image-based fluid transport modeling at the pore scale in geological materials: A practical introduction to the current state-of-the-art. *Earth-Science Reviews*, *155*, 93–128. https://doi.org/10.1016/j.earscirev.2016.02.001

Chauvet, F., Duru, P., Geoffroy, S., & Prat, M. (2009). Three periods of drying of a single square capillary tube. *Physical Review Letters*, *103*, 124502. https://doi.org/10.1103/PhysRevLett.103.124502

Crausse, P., Bacon, G., & Bories, S. (1981). Etude fondamentale des transferts couples chaleur-masse en milieu poreux. *International Journal of Heat and Mass Transfer*, *24*(6), 991–1004. https://doi.org/10.1016/0017-9310(81)90130-7

Gómez, I., Sala, J. M., & Millán, J. A. (2007). Characterization of moisture transport properties for lightened clay brick—Comparison between two manufacturers, *Journal of Building Physics*, *31*(2), 179–194. https://doi.org/10.1177/1744259107082687

He, W. S., Yi, J. S., & Van Nguyen, T. (2000). Two-phase flow model of the cathode of PEM fuel cells using interdigitated flow fields. *AIChE Journal*, *46*(10), 2053–2064. https://doi.org/10.1002/aic.690461016

Hoogland, F., Lehmann, P., Mokso, R., & Or, D. (2016). Drainage mechanisms in porous media: From piston-like invasion to formation of corner flow networks. *Water Resources Research*, *52*, 8413–8436. https://doi.org/10.1002/2016WR019299

Joekar-Niasar, V., & Hassanizadeh, S. M. (2011). Effect of fluids properties on non-equilibrium capillarity effects: Dynamic pore-network modeling. *International Journal of Multiphase Flow*, *37*(2), 198–214. https://doi.org/10.1016/j.ijmultiphaseflow.2010.09.007

Joekar-Niasar, V., Hassanizadeh, S. M., & Leijnse, A. (2008). Insights into the relationships among capillary pressure, saturation, interfacial area and relative permeability using pore-network modeling. *Transport in Porous Media*, *74*(2), 201–219. https://doi.org/10.1007/s11242-007-9191-7

Laurindo, J. B., & Prat, M. (1996). Numerical and experimental network study of evaporation in capillary porous media. Phase distributions. *Chemical Engineering Science*, *51*(23), 5171–5185. https://doi.org/10.1016/S0009-2509(96)00341-7

Laurindo, J. B., & Prat, M. (1998). Numerical and experimental network study of evaporation in capillary porous media. Drying rates. *Chemical Engineering Science*, *53*(12), 2257–2269. https://doi.org/10.1016/S0009-2509(97)00348-5

Le Bray, Y., & Prat, M. (1999). Three dimensional pore network simulation of drying in capillary porous media. *International Journal of Heat and Mass Transfer*, *42*, 4207–4224. https://doi.org/10.1016/S0017-9310(99)00006-X

Lehmann, P., Assouline, S., & Or, D. (2008). Characteristic lengths affecting evaporative drying of porous media. *Physical Review E*, *77*, 056309. https://doi.org/10.1103/PhysRevE.77.056309

Lerdahl, T. R., Øren, P. E., & Bakke, S. (2000). A predictive network model for three-phase flow in porous media, paper presented at the SPE/DOE Improved Oil Recovery Symposium. Tulsa, OK. https://doi.org/10.2118/59311-MS

Luikov, A. (1975). Systems of differential equations of heat and mass transfer in capillary-porous bodies (review). *International Journal of Heat and Mass Transfer*, *18*(1), 1–14. https://doi.org/10.1016/0017-9310(75)90002-2

Marchand, R. G., & Kumaran, M. K. (1994). Moisture diffusivity of cellulose insulation. *Journal of Thermal Insulation and Building Envelopes*, *17*, 362–377. https://doi.org/10.1177/109719639401700406

Metzger, T., Irawan, A., & Tsotsas, E. (2006). Remarks on the paper "Extension of Hoshen-Kopelman algorithm to non-lattice environments", By Al-Futaisi, A., Patzek, T. W. Physica A 321, 665–678 (2003), *Physica A*, *363*, 558–560. https://doi.org/10.1016/j.physa.2005.08.026

Metzger, T., Irawan, A., & Tsotsas, E. (2007a). Influence of pore structure on drying kinetics: A pore network study. *AIChE Journal*, *53*(12), 3029–3041. https://doi.org/10.1002/aic.11307

Metzger, T., Tsotsas, E., & Prat, M. (2007b). Pore network models: A powerful tool to study drying at the pore level and understand the influence of structure on drying kinetics. In A. Mujumdar & E. Tsotsas (Eds.), *Modern drying technology: Computational tools at different scales* (Vol. 1, pp. 57–102). Weinheim, Germany: Wiley.

Nowicki, S. C., Davis, H. T., & Scriven, L. (1992). Microscopic determination of transport parameters in drying porous media. *Drying Technology*, *10*, 925–946. https://doi.org/10.1080/07373939208916488

Øren, P. E., Bakke, S., & Arntzen, O. J. (1998). Extending predictive capabilities to network models. *SPE Journal*, *3*, 324–336. https://doi.org/10.2118/52052-PA

Pel, L., Brocken, H., & Kopinga, K. (1996). Determination of moisture diffusivity in porous media using moisture concentration profiles. *International Journal of Heat and Mass Tranfer*, *39*(6), 1273–1280. https://doi.org/10.1016/0017-9310(95)00201-4

Pel, L., Landman, K. A., & Kaasschieter, E. F. (2002). Analytic solution for the non-linear drying problem. *International Journal of Heat and Mass Tranfer*, *45*(15), 3173–3180. https://doi.org/10.1016/S0017-9310(02)00025-X

Perré, P., & Turner, I. W. (1999). A 3-D version of TransPore: A comprehensive heat and mass transfer computational model for simulating the drying of porous media. *International Journal of Heat and Mass Transfer*, *42*(24), 4501–4521. https://doi.org/10.1016/S0017-9310(99)00098-8

Philip, J. R., & De Vries, D. A. (1957). Moisture movement in porous materials under temperature gradients. *Eos, Transactions American Geophysical Union*, *38*(2), 222–232. https://doi.org/10.1029/TR038i002p00222

Prat, M. (1991). 2D Modelling of drying of porous media: Influence of edge effects at the interface. *Drying Technology*, *9*(5), 1181–1208. https://doi.org/10.1080/07373939108916748

Prat, M. (2002). Recent advances in pore-scale models for drying of porous media. *Chemical Engineering Journal*, *86*, 153–164. https://doi.org/10.1016/S1385-8947(01)00283-2

Prat, M. (2007). On the influence of pore shape, contact angle and film flows on drying of capillary porous media. *International Journal of Heat and Mass Transfer*, *50*, 1455–1468. https://doi.org/10.1016/j.ijheatmasstransfer.2006.09.001

Pujol, A., Debenest, G., Pommier, S., Quintard, M., & Chenu, D. (2011). Modeling composting processes with local equilibrium and local non-equilibrium approaches for water exchange terms. *Drying Technology*, *29*(16), 1941–1953. https://doi.org/10.1080/07373937.2011.599506

Quintard, M., & Whitaker, S. (1993). One-and two-equation models for transient diffusion processes in two-phase systems. *Advances in Heat Transfer*, *23*, 369–464. https://doi.org/10.1016/S0065-2717(08)70009

Quintard, M., & Whitaker, S. (1994). Convection, dispersion, and interfacial transport of contaminants: Homogeneous porous media. *Advances in Water Resources*, *17*, 221–239. https://doi.org/10.1016/0309-1708(94)90002-7

Sahimi, M. (2011). *Flow and transport in porous media and fractured rock: From classical methods to moden approaches* (2nd ed.). New York, NY: Wiley.

Schoeber, W. (1976). *Regular regimes in sorption processes: Calculation of drying rates and determination of concentration dependent diffusion coefficients* (PhD thesis). Eindhoven, the Netherlands: Technical University.

Schrage, R. W. (1953). *A theoretical study of interphase mass transfer* (PhD thesis). New York, NY: Columbia University Press.

Tahmasebi, P., Sahimi, M., Kohanpur, A. H., & Valocchi, A. (2017). Pore-scale simulation of flow of CO_2 and brine in reconstructed and actual 3D rock cores. *Journal of Petroleum Science and Engineering*, *155*, 21–33. https://doi.org/10.1016/j.petrol.2016.12.031

Vorhauer, N., Metzger, T., & Tsotsas, E. (2010). Extraction of effective parameters for continuous drying model from discrete pore network model, paper presented at *17th International Drying Symposium*, Magdeburg, Germany.

Vorhauer, N., Wang, Y. J., Kharaghani, A., Tsotsas, E., & Prat, M. (2015). Drying with formation of capillary rings in a model porous medium. *Transport in Porous Media*, *110*(2), 197–223. https://doi.org/10.1007/s11242-015-0538-1

Wang, Y., Kharaghani, A., Metzger, T., & Tsotsas, E. (2012). Pore network drying model for particle aggregates: Assessment by X-Ray microtomography. *Drying Technology*, *30*(15), 1800–1809. https://doi.org/10.1080/07373937.2012.713422

Whitaker, S. (1977). Simultaneous heat, mass, and momentum transfer in porous media: A theory of drying. *Advances in Heat Transfer*, *13*, 119–203. https://doi.org/10.1016/S0065-2717(08)70223-5

Yiotis, A. G., Boudouvis, A. G., Stubos, A. K., Tsimpanogiannis, I. N., & Yortsos, Y. C. (2004). Effect of liquid films on the drying of porous media. *AIChE Journal*, *50*, 2721–2731. https://doi.org/10.1002/aic.10265

Yiotis, A. G., Salin, D., Tajer, E. S., & Yortsos, Y. C. (2012). Drying in porous media with gravity-stabilized fronts: Experimental results. *Physical Review E*, *86*, 026310. https://doi.org/10.1103/PhysRevE.86.026310